Desulfovibrio magneticus RS-1 contains an iron- and phosphorus-rich organelle distinct from its bullet-shaped magnetosomes

Meghan E. Byrne[a], David A. Ball[b,1], Jean-Luc Guerquin-Kern[c,d,1], Isabelle Rouiller[e,f], Ting-Di Wu[c,d], Kenneth H. Downing[b], Hojatollah Vali[e,f,g], and Arash Komeili[a,2]

[a]Department of Plant and Microbial Biology, University of California, Berkeley, CA 94720; [b]Lawrence Berkeley National Laboratory, Berkeley, CA 94720; [c]Institut National de la Santé et de la Recherche Médicale, U759, 91405 Orsay, France; [d]Institut Curie, Laboratoire de Microscopie Ionique, 91405 Orsay, France; and [e]Facility for Electron Microscopy Research, [f]Department of Anatomy and Cell Biology, and [g]Department of Earth and Planetary Sciences, McGill University, Montreal, QC, Canada H3A 2B2

Edited by Caroline S. Harwood, University of Washington, Seattle, WA, and approved May 17, 2010 (received for review February 2, 2010)

Intracellular magnetite crystal formation by magnetotactic bacteria has emerged as a powerful model for investigating the cellular and molecular mechanisms of biomineralization, a process common to all branches of life. Although magnetotactic bacteria are phylogenetically diverse and their crystals morphologically diverse, studies to date have focused on a few, closely related species with similar crystal habits. Here, we investigate the process of magnetite biomineralization in *Desulfovibrio magneticus* sp. RS-1, the only reported species of cultured magnetotactic bacteria that is outside of the α-Proteobacteria and that forms bullet-shaped crystals. Using a variety of high-resolution imaging and analytical tools, we show that RS-1 cells form amorphous, non-crystalline granules containing iron and phosphorus before forming magnetite crystals. Using NanoSIMS (dynamic secondary ion mass spectroscopy), we show that the iron-phosphorus granules and the magnetite crystals are likely formed through separate cellular processes. Analysis of the cellular ultrastructure of RS-1 using cryo-ultramicrotomy, cryo-electron tomography, and tomography of ultrathin sections reveals that the magnetite crystals are not surrounded by membranes but that the iron-phosphorus granules are surrounded by membranous compartments. The varied cellular paths for the formation of these two minerals lead us to suggest that the iron-phosphorus granules constitute a distinct bacterial organelle.

bacterial organelle | biomineralization | magnetotactic bacteria | dynamic secondary ion mass spectroscopy | magnetite

Biomineralization, the biologically controlled transformation of inorganic compounds into highly-ordered structures, is performed by organisms in all branches of life, from bacteria to humans. Because biogenic minerals often have superior properties to their chemically synthesized counterparts, understanding biomineralization is important to fields as diverse as inorganic materials synthesis and medicine (1, 2). Among the numerous organisms capable of biomineralization, magnetotactic bacteria (MB), a group of microbes that form intracellular chains of magnetic minerals including magnetite and greigite, have become powerful models for studying biomineralization because of their relatively fast growth rate and genetic tractability (3).

Investigation of the cellular ultrastructure of MB has shown that the magnetite crystals are formed within membranous intracellular compartments called magnetosomes, which are present before the formation of magnetite (4, 5). Other studies have shown that when magnetite formation is induced by decreasing oxygen levels or adding iron to iron-deprived cells, multiple crystals in the chain nucleate simultaneously (5, 6). These insights into the kinetics of magnetite biomineralization have been complemented by molecular studies. A genomic island called the magnetosome island (MAI) has been found in all MB studied to date. Loss of the MAI results in an absence of magnetosome membranes and magnetite crystals, and genes found in the MAI have been shown to play a role in the formation of the magnetite crystals and the magnetosome chain (7).

Although knowledge of magnetite biomineralization is growing, our current understanding is based on studies of a relatively narrow subset of magnetotactic bacterial strains. All studies cited above have focused on MB that belong to the α-Proteobacteria and form magnetite crystals with octahedral or hexahedral habits (1). However, MB have been identified in at least four phylogenetic branches of bacteria and have been found to exhibit a large diversity of crystal morphologies, including octahedral, prismatic, "tooth-shaped," and "bullet-shaped" crystals (8–10). To know the full spectrum of mechanisms that have evolved to direct magnetite biomineralization, an examination of other magnetotactic bacterial species is needed.

Desulfovibrio magneticus sp. RS-1 (RS-1) is an ideal system to investigate the range of magnetite biomineralization mechanisms used by MB, because it is the only axenically cultured magnetotactic bacterium outside of the α-Proteobacteria and forms crystals that are irregular or bullet-shaped (11–13). Recently, the genome of RS-1 was sequenced and found to contain a region resembling a highly edited version of the MAI (14, 15). Many of the genes in the RS-1 MAI are highly divergent from their homologs in the magnetotactic α-Proteobacteria, and a number of the genes thought to be important for crystal growth and morphology are absent, raising the question of whether RS-1 has evolved a divergent mechanism of magnetite biomineralization. However, biomineralization in RS-1 has been difficult to investigate because of the strain's weak magnetotactic behavior, corresponding with the production of relatively few, small magnetic crystals that show "superparamagnetic-like" behavior (16, 17).

The goal of this work is to identify growth conditions that increase RS-1's magnetotactic behavior, to define the steps of magnetite biomineralization in RS-1 and the cellular context in which biomineralization occurs. Using a number of analytical and imaging techniques, we show that RS-1 cells contain membranous granules rich in iron and phosphorus that are distinct from their bullet-shaped magnetite crystals. Additionally, we present evi-

MICROBIOLOGY

Author contributions: M.E.B., H.V., and A.K. designed research; M.E.B., D.A.B., J.-L.G.-K., I.R., T.-D.W., and H.V. performed research; M.E.B., D.A.B., J.-L.G.-K., I.R., T.-D.W., and H.V. contributed new reagents/analytic tools; M.E.B., D.A.B., J.-L.G.-K., I.R., T.-D.W., K.H.D., H.V., and A.K. analyzed data; and M.E.B. and A.K. wrote the paper.

The authors declare no conflict of interest.

This article is a PNAS Direct Submission.

Freely available online through the PNAS open access option.

[1]D.A.B. and J.-L.G.-K. contributed equally to this work.

[2]To whom correspondence should be addressed. E-mail: komeili@berkeley.edu.

This article contains supporting information online at www.pnas.org/lookup/suppl/doi:10.1073/pnas.1001290107/-/DCSupplemental.

dence that, in contrast to other MB, a lipid-bilayer membrane does not surround the magnetosomes of RS-1.

Results

This study initially focused on optimizing the growth of RS-1 to increase the magnetic properties of the cells. The magnetic behavior of a culture of MB is often determined via its Cmag value, which is the ratio of a culture's maximal to its minimal optical density as cells rotate in a turning magnetic field, and it has been shown to serve as a reliable proxy for the average number of single-domain magnetite crystals formed per cell (18). RS-1 cultures grown under standard conditions have Cmag values of 1.02 to 1.05 and, accordingly, only 30 to 50% of the cells contain crystals. By optimizing various aspects of the growth medium, the Cmag values increased to 1.40 to 1.60 and 100% of cells contained crystals ranging in size from 32–85 nm (see *SI Results* and Fig. S1 for more information).

The process of magnetite biomineralization in RS-1 was then explored by examining magnetite formation following iron uptake in iron-starved cells. Cultures of RS-1 were passaged several times in medium without iron to obtain cells that lacked magnetite crystals. These cells did not turn in a magnetic field (Cmag = 1.00) and were free of magnetite crystals as verified by transmission electron microscopy (TEM) (Fig. 1, 0 h). Ferric malate (100 μM) was then added to cultures in early exponential growth, and the cells were visualized by TEM at different time points after iron addition. As early as 15 min following iron addition, round, electron-dense granules, not organized in chains, were visible throughout the cells. The granules reached a maximum number of 145 ± 31 per cell 3 h after iron addition and then decreased in number at a rate faster than would be expected if they were merely diluted through cell division, until almost none were visible 50 to 70 h after iron addition (Fig. 1 and Fig. S2*A*). Cells containing these granules did not turn in a rotating magnetic field or bind to magnetic columns sensitive to superparamagnetic iron particles, indicating that the granules are not magnetic. After 21 to 24 h, the cells began to turn in a rotating magnetic field and bullet-shaped crystals became visible by TEM (Fig. 1 and Fig. S2*B*). Instead of a complete chain of nucleating crystals appearing simultaneously, as has been seen in other MB (5), most RS-1 cells had only one to two crystals initially. The average number of crystals increased with time, which correlated with an increase in the cultures' Cmag readings, until there was an average of 13 to 15 crystals per cell after 50 h of growth in iron (Fig. S2*B*).

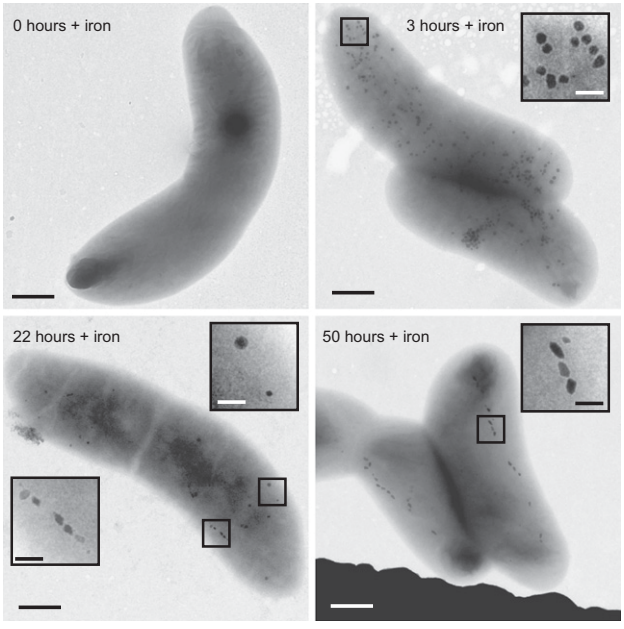

Fig. 1. RS-1 forms round granules before magnetite crystals after the addition of iron to iron-starved cells. Transmission electron micrographs of RS-1 cells at various times after iron addition. At time 0, before iron addition, no magnetite crystals or granules are visible. Three hours after iron addition, round granules (enlarged in *Inset*) are present throughout the cytoplasm. Twenty-two hours after iron addition, granules (*Upper Right Inset*) are still present and magnetite crystals (*Lower Left Inset*) begin to appear. Fifty hours after iron addition, almost no granules remain and chains of magnetite crystals (enlarged in *Inset*) are present. [Scale bars = 500 nm and 100 nm (*Insets*).]

The granules that appeared transiently following iron addition have not previously been reported to form in MB. To determine the structure and chemical composition of the electron-dense granules, energy-dispersive X-ray spectroscopy (EDS) and high-resolution TEM (HRTEM) were performed on RS-1 cells. EDS analysis revealed that the round granules contain iron, oxygen, and phosphorus, whereas the magnetite crystals contain iron and oxygen only (Fig. S3). HRTEM imaging showed that although the bullet-shaped magnetite particles were crystalline as expected (Fig. S4*A*), the round granules lacked an obvious crystalline lattice and were in fact amorphous (Fig. S4*B*). In all iron-addition experiments, the iron-phosphorus (Fe-P) granules formed before the magnetite crystals, raising the possibility that they were precursors to the magnetite crystals.

To address the possibility that the granules transform into magnetite, a pulse-chase experiment was conducted (Fig. 2). ^{56}Fe, in the form of naturally occurring iron (92% ^{56}Fe), was given to iron-starved RS-1 cells in early exponential growth. After 3 h, they were washed and transferred to medium containing ^{57}Fe (94% purity) as the sole iron source. Cells were then collected at various times, sectioned, and visualized by TEM and dynamic secondary ion mass spectroscopy (NanoSIMS), a powerful technology that allows spatial imaging of elemental and isotopic distribution with a resolution of less than 100 nm (Fig. 2). The addition of ^{57}Fe did not affect the growth rate of RS-1 cells (10–11 h doubling time under all conditions), the number of magnetite crystals per cell, or the final Cmag of the cultures, suggesting that the cells use both iron isotopes equally well. If the Fe-P granules were direct precursors of the magnetite crystals, then the magnetite crystals would be expected to contain amounts of ^{56}Fe similar to the granules.

The NanoSIMS analysis showed that after 3 h of growth in ^{56}Fe medium, strong ^{56}Fe spots were present where Fe-P granules could be seen by TEM (Fig. 2*A*). Given the ubiquitous presence of phosphorus-containing organic molecules, the entire cellular space emits a faint ^{31}P signal. And, as expected from the EDS analysis, the Fe-P granules appear as strong ^{31}P spots over this faint background that colocalize with the ^{56}Fe spots (Fig. 2*A*). Cells grown in medium containing ^{56}Fe for 3 h and subsequently transferred to medium containing ^{57}Fe for 18.5 h began to turn in a magnetic field. These cells possess a few magnetite crystals as revealed by TEM that contained primarily ^{57}Fe (Fig. 2*B*), but the NanoSIMS images of areas containing Fe-P granules revealed the presence of both ^{56}Fe and ^{57}Fe (Fig. 2*C*). These results strongly suggested that the granules are not direct precursors of the magnetite crystals. This hypothesis was bolstered by data from crystals formed after 3 h in ^{56}Fe followed by 47 h in ^{57}Fe. At this time point, almost no Fe-P granules were detected by TEM and a large number of clearly identifiable magnetite crystals could be observed. Most of these crystals had strong ^{57}Fe signals (Fig. 2*D*), which further supports the idea that the granules formed in the first 3 h after iron addition do not transform directly into magnetite crystals. There were, however, chains of magnetite in some bacteria that contained relatively small amounts of ^{56}Fe (Fig. 2*D*). Some of the iron used to form these magnetite crystals likely came from the dissolution of the granules. It is also possible the background levels of ^{56}Fe in the ^{57}Fe preparation could make a disproportionate contribution to

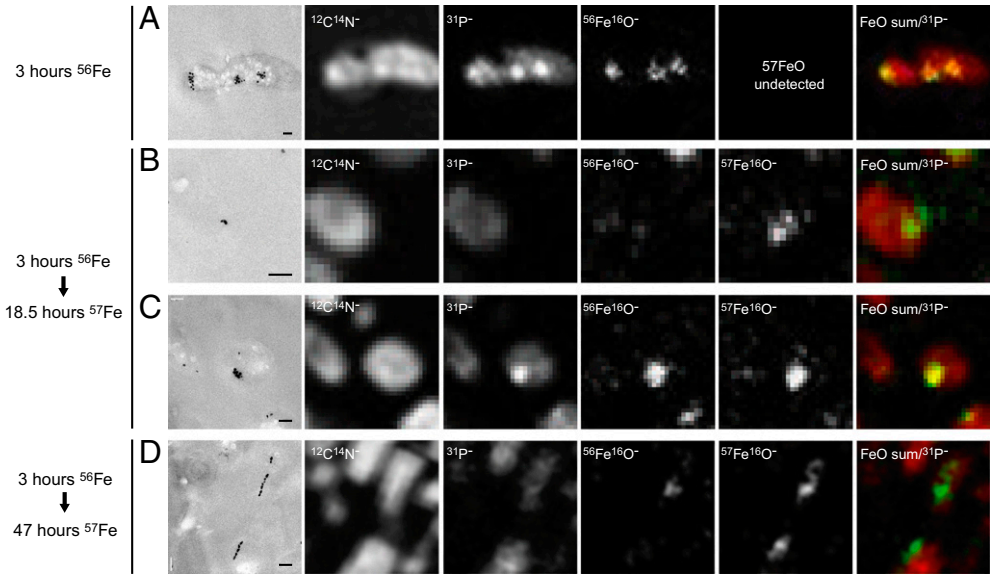

Fig. 2. NanoSIMS analysis of biomineralization in RS-1. Iron-starved RS-1 cells were given 200 μM ferric (^{56}Fe) malate for 3 h, then transferred to medium containing 200 μM ferric (^{57}Fe) malate. At each time point, thin sections of cells were imaged by TEM (*Far Left*) and analyzed by NanoSIMS for $^{12}C^{14}N^-$, $^{31}P^-$, $^{56}Fe^{16}O^-$, and $^{57}Fe^{16}O^-$. The CN and P signals indicate the presence of ubiquitous organic molecules and thus highlight the entire cellular space. When present, the Fe-P granules emit a strong ^{31}P signal over the fainter background signal. The far-right panels show a dual merge of the sum of both FeO^- signals (green) and the $^{31}P^-$ signal (red). (*A*) Fe-P granules in a cell grown with ^{56}Fe for 3 h. (*B*) A single magnetite crystal in a cell grown with ^{56}Fe for 3 h then ^{57}Fe for 18.5 h. (*C*) A cluster of Fe-P granules in a cell grown with ^{56}Fe for 3 h then ^{57}Fe for 18.5 h. (*D*) A chain of magnetite crystals in a cell grown with ^{56}Fe for 3 h then ^{57}Fe for 47 h. (Scale bars, 200 nm.)

these magnetite crystals, although iron isotope fractionation has not been observed in other MB (19).

The NanoSIMS results suggested that the Fe-P granules and the magnetite crystals are formed through separate cellular processes. To investigate the connections between these two iron-rich inclusions, cryo-ultramicrotomy followed by electron microscopy was used to identify the cellular context in which magnetite crystals and Fe-P granules are formed in RS-1. Cryo-ultramicrotomy allows for a more faithful preservation of cellular structures during sectioning and sample preparation for electron microscopy. When used in imaging other MB, this technique can distinguish empty magnetosome membranes from other cellular structures (5). TEM study of the cryo-ultrathin sections showed that the cytoplasm of RS-1 cells was filled with intracellular compartments (Fig. 3). Unlike magnetosome membranes, these intracellular compartments were not aligned in a chain, and small crystals nucleating and growing within the membranous compartments were not observed. In fact, TEM of cryo-ultrathin sections stained with uranyl oxalic acid in water (0.3 M) for 5 min and cryo-protected from drying by a thin film of 2% methylcellulose containing 4% uranyl acetate showed that the density of the material inside these vesicles is similar to the material within the periplasmic space.

RS-1 forms small crystals that are idiomorphous or diamond-shaped and larger crystals that are bullet-shaped (Fig. S4*B*). If biomineralization proceeded in the same manner as in the magnetotactic α-Proteobacteria, these smaller diamond-shaped crystals should reside in compartments that resemble the mature bullet-shaped crystals. Yet, no small crystals of any kind were observed within larger membranous compartments described above. Although we did observe halos surrounding the crystals at extreme underfocus conditions, an enveloping membrane around the magnetite crystals could not be detected (Fig. 3 *C* and *D*, and Fig. S5). Thus, in contrast to other MB, the magnetite crystals of RS-1 do not reside within membranous compartments.

Cryo-electron tomography (CET) was used to further investigate the intracellular membranous compartments and their relationship with the magnetite crystals and Fe-P granules. CET allows the visualization of the 3D ultrastructure of small (ideally less than 500 nm thick) cells in a near-native or "frozen hydrated" state (20). This technique has been used previously to

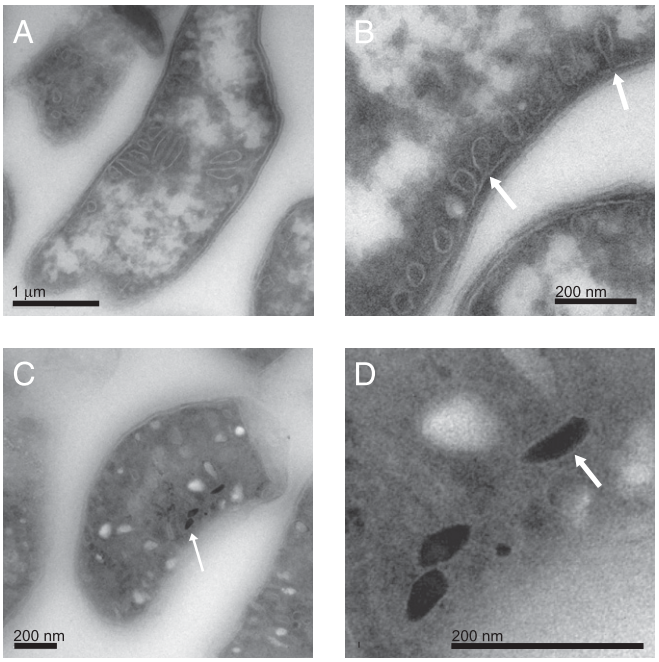

Fig. 3. RS-1 contains numerous and varied intracellular membranous compartments. (*A* and *B*) TEM images of cryo-ultrathin sections of RS-1 cells grown in iron-free medium. (*B*) Arrows highlight invaginations of the inner membrane. (*C*) Cryo-ultrathin sections of RS-1 cells, grown for 24 h in medium with iron. Arrows highlight magnetite crystals. (*D*) Enlargement of crystals from *C*. Arrow highlights halo seen around some crystals in underfocus conditions.

observe magnetosome membranes, including those that are filled with mature magnetite crystals (21). Three-dimensional reconstructions of intact cells revealed internal structures and invaginations of the inner membrane, but the overall thickness of the RS-1 cells (800 nm to 1 μm) prevented clear visualization of these structures (Fig. S6). To overcome this obstacle, the cells were gently lysed by freezing and thawing to decrease their diameter. The reconstructed tomograms of the partially lysed RS-1 cells showed intracellular structures similar to what was seen by cryo-ultramicrotomy, including elongated compartments (Fig. 4*C*), invaginations of the inner membrane (Fig. 4*D*), and round vesicles (Fig. 4 *D* and *E* and Movie S1). CET also revealed membranes around the Fe-P granules (Fig. 4*A*), but none were apparent around the magnetite crystals (Fig. 4*B*). Although we observed a halo-effect around the magnetite crystals that presumably might obscure membranes, this bright signal was also present around the Fe-P granules where membranes could clearly be seen.

Finally, we used a third high-resolution microscopic technique to image the ultrastructure of RS-1 cells. Electron tomography of cryo-ultrathin sections of a fixed RS-1 cell revealed intracellular compartments similar to what had been observed through CET of whole cells, including long tubular compartments at the periphery of the cell (Fig. 5*A*). However, a series of 7-nm-thick tomographic *x-y* slices through the magnetite crystals revealed no membranes around the crystals. This observation was made clearer by superposing 3D reconstructions of the magnetite crystals on a central slice of the volume (Fig. 5*C*). The crystals are directly adjacent to each other, with no surrounding bilayer membranes.

Together, these microscopic analyses revealed that the Fe-P granules and the magnetite crystals clearly were localized within different parts of the cellular ultrastructure, further supporting the conclusion that they are formed through independent cellular processes.

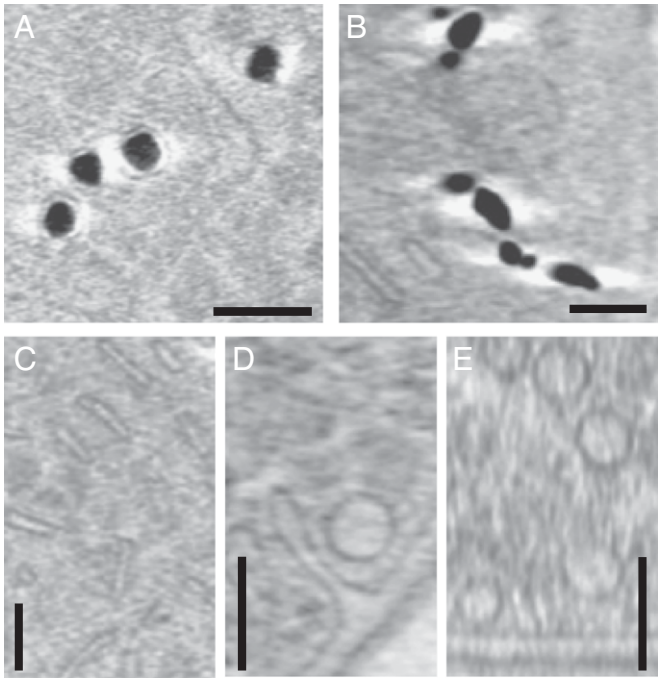

Fig. 4. Cryo-electron microscopy of fully hydrated cells reveals intracellular membranous compartments and membranes around the Fe-P granules, but no membranes are visible around the magnetite crystals. Images are 19.2-nm thick sections taken from reconstructed cryo-electron tomograms. (*A*) Fe-P inclusions from a cell grown in medium with iron for 4.5 h. (*B*) Magnetite crystals from a cell grown in medium with iron for 56 h. (*C*) Thin, elongated compartments. (*D*) An invagination of the inner membrane and a round vesicle. (*E*) Multiple round vesicles. (Scale bars, 100 nm.)

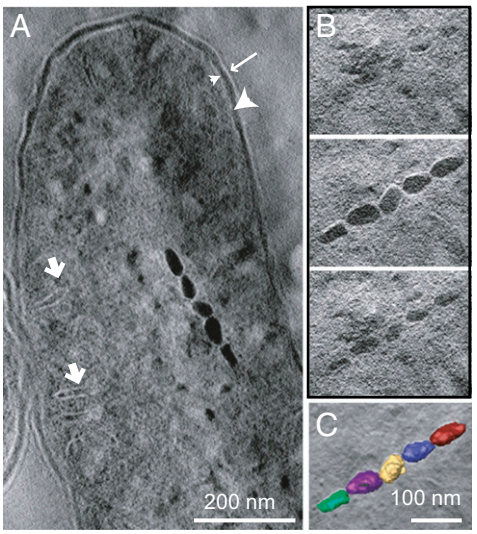

Fig. 5. Electron tomography analysis of a section of RS-1, grown for 96 h with iron, shows a chain of magnetite crystals with no membranes. (*A*) A tomographic *x-y* slice of ~40 nm thickness of the bacteria. Highlighted are part of the magnetosome chain, outer membrane (long arrow), periplasmic space (large arrowhead), inner membrane (small arrowhead), and intracellular membrane compartments (short arrows). (*B*) A series of tomographic *x-y* slices of ~7 nm thickness from bottom to top of the magnetosome chain. (*C*) The magnetosome chain superposed with a central section of the volume. The volume was manually segmented using IMOD, and each magnetosome was given a different color.

Discussion

In this study, we examined the process of magnetite crystal biomineralization in RS-1, a strain of MB that forms bullet-shaped magnetite crystals and is a member of the δ-Proteobacteria. Our results revealed a number of unusual features that necessitate a reexamination of the mechanisms of biomineralization in this organism. Following the addition of iron to iron-starved cells, RS-1 formed noncrystalline, iron- and phosphorus-containing granules within membranous compartments. The Fe-P granules were transient, and few granules could be seen in RS-1 cells grown continuously in iron-containing medium, similar to what was seen in cells 50 h after iron addition. This finding suggests that the granules form in response to an influx of iron and then disappear as the cells reach iron homeostasis. The Fe-P granules may be formed for the purpose of iron storage or for the sequestration of iron, which otherwise might be present at toxic concentrations within the cytoplasm following a large influx of iron.

With the recent development of high-resolution ion probes, such as NanoSIMS, SIMS techniques have been increasingly applied to biological systems (22). In this study, we demonstrated the utility of this technique in examining the spatial progress of biomineralization. This technique provided evidence that the Fe-P granules are not direct precursors of the magnetite crystals. This finding is supported by observations that the Fe-P granules are not sufficient to allow magnetite formation if cells grown transiently in iron-rich conditions are transferred to "no iron" conditions (*SI Results*). In addition, using CET we observed that the Fe-P granules are formed within membranous compartments although the magnetite crystals, observed by multiple microscopic techniques, appear to be free of membranes. Together, these results suggest that the Fe-P granules and the magnetite crystals form through distinct cellular processes, suggesting that the compartment containing the Fe-P granules constitutes

a bacterial organelle. Interestingly, RS-1 forms extensive intracellular membranous structures, not only round vesicles but also narrow, elongated compartments. Future work must be done to determine if these two types of membranous compartments represent different growth stages of the same structure, or if they are separate structures with distinct cellular functions.

Although *Desulfovibrio* have traditionally been studied for their role in biocorrosion of metals and the souring of oil fields they also may have applications in the bioremediation of toxic compounds and the recovery of precious metals (23). Combining the industrial function of *Desulfovibrio* with a magnetic phenotype could well increase their usefulness. In addition, understanding the ultrastructure of *Desulfovibrio* may help to refine the biotechnological application of these bacteria. To our knowledge, this study is unique in showing extensive intracellular membranes within a *Desulfovibrio*. However, *Desulfovibrio gigas* has been found to form electron-dense, round granules containing large amounts of P, K, and Mg under Fe^{2+}- or NH_4^+-limited conditions (24), implying that this class of organelles may be common to multiple strains of *Desulfovibrio*.

Magnetosome membranes have been observed around the magnetite crystals formed in all α-Proteobacterial MB studied to date. And a previous report has implied that purified magnetite crystals from RS-1 appear to be surrounded by a diffuse organic layer (25). However, we believe that this finding may be an artifact of the imaging technique used. These findings are also confounded by the presence of numerous organic contaminants in the magnetosome fractions of RS-1 that may bind to the crystals and give the appearance of a membrane layer. Other than their appearance, the behavior of purified RS-1 magnetite particles also implies a different mode of organization of magnetosomes in this organism. Once isolated, RS-1 crystals tend to collapse into large aggregates (Fig. S1) (25). In contrast, magnetite crystals isolated from the magnetotactic α-Proteobacteria remain in chains and aggregate only after being treated with detergents that dissolve the magnetosome membrane (26, 27). For these reasons, we used three different high-resolution microscopic techniques to investigate the presence of a magnetosome membrane in vivo. Surprisingly, all of these approaches showed that magnetite crystals in RS-1 are not surrounded by membranes.

This conclusion is significant because the magnetosome membrane is thought to be important for the localization of a specific cohort of proteins that are critical for the formation of magnetite crystals. However, an examination of RS-1's potential magnetosome genes further supports our findings. The recently sequenced genome of RS-1 encodes for homologs of 10 of the known magnetosome proteins that are thought to be important for magnetosome formation in the magnetotactic α-Proteobacteria (14). However, some of the genes known to be involved in crucial steps of magnetosome formation are missing from the RS-1 genome. For instance, *mamI* and *mamL*, two genes that are essential for the formation of the magnetosome membrane and are present exclusively in MB, are missing from the RS-1 genome (28). Furthermore, *mamGFDC* and *mms6*, which play roles in regulation of crystal size and shape, are also missing from RS-1 (29, 30). Of the genes that are present some, such as *mamM*, appear to encode proteins with transmembrane domains, raising the possibility that some stage of biomineralization in RS-1 may be associated with cellular membranes. Perhaps, RS-1 crystals are only transiently associated with membranes and are released once they mature. We also cannot rule out the possibility that membranes are so tightly associated with these crystals that they cannot be imaged by high-resolution microscopic techniques used in this study. Finally, it is possible that bullet-shaped crystals, as a class, are not formed within magnetosome membranes. Hanzlik et al. previously reported in a study of *Magnetotactic bavaricum*, a bacterium that also forms bullet-shaped crystals, that they were not able to detect membranes around the crystals, even after using multiple sample preparation techniques (31).The intriguing differences between RS-1 and the magnetotactic α-Proteobacteria established by this and other studies demonstrate that further investigation of the molecular mechanisms of magnetite formation in divergent species of MB is needed before a deeper understanding of the evolution of biomineralization can be achieved.

Materials and Methods

Growth Conditions and Medium Composition. *D. magneticus* sp. RS-1 was obtained from the German Collection of Microorganisms and Cell Cultures (DSMZ) (DSM no. 13731) and grown in a modified version of the DSMZ's "*Desulfovibrio magneticus* medium," here called "RS-1 growth medium" (11). Before inoculating with cells, Wolfe's vitamins (0.8% total volume), 20 mM ferric malate (100 μM final), and 28.5 mM cysteine-HCl (285 μM final) were added, and the medium was bubbled with nitrogen gas again. For details, see *SI Materials and Methods*.

Whole-Cell TEM. Cells were placed on copper grids coated with 0.5% formvar in ethylene dichloride and incubated for 5 min, after which the grids were washed three times in distilled, de-ionized water and dried. No stain was used. For details, see *SI Materials and Methods*.

Cryo-Ultramicrotomy and CET. Cells were collected by centrifugation at 8,000 × *g* for 10 min or filtering, washed twice in 1 mL, 1 mM PBS, layered with 1 mL 2.5% glutaraldehyde in PBS, and stored at 4 °C. Cryo-fixation and cryo-ultramicrotomy were performed as previously described (5). For details, see *SI Materials and Methods*.

NanoSIMS. SIMS imaging was performed using a NanoSIMS-50 Ion Microprobe (CAMECA) operating in scanning mode (32, 33). The elemental mapping was performed on the same thin section previously observed by TEM. For details, see *SI Materials and Methods*.

ACKNOWLEDGMENTS. We thank Kent McDonald and Reena Zalpuri of the University of California Berkeley Electron Microscope Laboratory for technical assistance; members of John Coates' laboratory for technical assistance and equipment; and Olga Draper, Shannon Greene, Sepehr Keyhani, Dorothée Murat, and Anna Quinlan for critical reading of the manuscript. We also thank the PICT-IBiSA imaging facility in the Institut Curie and J. Mui and Dr. S. K. Sears (both of the Facility for Electron Microscopy Research, McGill University) for assistance. A.K. is supported by a grant through the David and Lucille Packard Foundation. H.V. acknowledges financial support from the Natural Sciences and Engineering Research Council (NSERC) of Canada. I.R. received funding from NSERC (Grant 355873-08) as well as the receipt of a Canadian Institutes of Health Research New Investigator award. This work was supported in part by US Department of Energy Contract DE-AC02-05CH11231.

1. Bazylinski DA, Frankel RB (2004) Magnetosome formation in prokaryotes. *Nat Rev Microbiol* 2:217–230.
2. Crookes-Goodson WJ, Slocik JM, Naik RR (2008) Bio-directed synthesis and assembly of nanomaterials. *Chem Soc Rev* 37:2403–2412.
3. Komeili A (2007) Molecular mechanisms of magnetosome formation. *Annu Rev Biochem* 76:351–366.
4. Gorby YA, Beveridge TJ, Blakemore RP (1988) Characterization of the bacterial magnetosome membrane. *J Bacteriol* 170:834–841.
5. Komeili A, Vali H, Beveridge TJ, Newman DK (2004) Magnetosome vesicles are present before magnetite formation, and MamA is required for their activation. *Proc Natl Acad Sci USA* 101:3839–3844.
6. Schüler D, Baeuerlein E (1998) Dynamics of iron uptake and Fe3O4 biomineralization during aerobic and microaerobic growth of *Magnetospirillum gryphiswaldense*. *J Bacteriol* 180:159–162.
7. Ullrich S, Kube M, Schübbe S, Reinhardt R, Schüler D (2005) A hypervariable 130-kilobase genomic region of *Magnetospirillum gryphiswaldense* comprises a magnetosome island which undergoes frequent rearrangements during stationary growth. *J Bacteriol* 187: 7176–7184.
8. Lins U, Freitas F, Keim CN, Farina M (2000) Electron spectroscopic imaging of magnetotactic bacteria: Magnetosome morphology and diversity. *Microsc Microanal* 6: 463–470.
9. Vali H, Kirschvink JL (1990) Observations of magnetosome organization, surface structure, and iron biomineralization of undescribed magnetic bacteria: Evolutionary speculations. *Iron Biominerals*, eds Frankel RB, Blakemore RP (Plenum Press, New York), pp 97–115.
10. Amman R, Peplies J, Schuler D (2007) *Diversity and Taxonomy of Magnetotactic Bacteria.* Microbiology Monographs (Springer, Berlin, Heidelberg), Vol 3, pp 25–36.

11. Sakaguchi T, Burgess JG, Matsunaga T (1993) Magnetite formation by a sulfate-reducing bacterium. *Nature* 365:47–49.
12. Sakaguchi T, Arakaki A, Matsunaga T (2002) *Desulfovibrio magneticus* sp. nov., a novel sulfate-reducing bacterium that produces intracellular single-domain-sized magnetite particles. *Int J Syst Evol Microbiol* 52:215–221.
13. Kawaguchi R, et al. (1995) Phylogenetic analysis of a novel sulfate-reducing magnetic bacterium, RS-1, demonstrates its membership of the delta-Proteobacteria. *FEMS Microbiol Lett* 126:277–282.
14. Nakazawa H, et al. (2009) Whole genome sequence of *Desulfovibrio magneticus* strain RS-1 revealed common gene clusters in magnetotactic bacteria. *Genome Res* 19: 1801–1808.
15. Arakaki A, Masuda F, Amemiya Y, Tanaka T, Matsunaga T (2010) Control of the morphology and size of magnetite particles with peptides mimicking the Mms6 protein from magnetotactic bacteria. *J Colloid Interface Sci* 343:65–70.
16. Sakaguchi T, Tsujimura N, Matsunaga T (1996) A novel method for isolation of magnetic bacteria without magnetic collection using magnetotaxis. *J Microbiol Methods* 26:139–145.
17. Posfai M, et al. (2006) Properties of intracellular magnetite crystals produced by *Desulfovibrio magneticus* strain RS-1. *Earth Planet Sci Lett* 249:444–455.
18. Schuler D, Uhl R, Bauerlein E (1995) A simple light-scattering method to assay magnetism in *Magnetospirillum gryphiswaldense*. *FEMS Microbiol Lett* 132:139–145.
19. Mandernack KW, Bazylinski DA, Shanks WC, 3rd, Bullen TD (1999) Oxygen and iron isotope studies of magnetite produced by magnetotactic bacteria. *Science* 285: 1892–1896.
20. Kürner J, Medalia O, Linaroudis AA, Baumeister W (2004) New insights into the structural organization of eukaryotic and prokaryotic cytoskeletons using cryo-electron tomography. *Exp Cell Res* 301:38–42.
21. Komeili A, Li Z, Newman DK, Jensen GJ (2006) Magnetosomes are cell membrane invaginations organized by the actin-like protein MamK. *Science* 311:242–245.
22. Boxer SG, Kraft ML, Weber PK (2009) Advances in imaging secondary ion mass spectrometry for biological samples. *Annu Rev Biophys* 38:53–74.
23. Barton LL, Fauque GD (2009) Biochemistry, physiology and biotechnology of sulfate-reducing bacteria. *Adv Appl Microbiol* 68:41–98.
24. Hensgens CMH, Santos H, Zhang C, Kruizinga WH, Hansen TA (1996) Electron-dense granules in *Desulfovibrio gigas* do not consist of inorganic triphosphate but of a glucose pentakis(diphosphate). *Eur J Biochem* 242:327–331.
25. Matsunaga T, Nemoto M, Arakaki A, Tanaka M (2009) Proteomic analysis of irregular, bullet-shaped magnetosomes in the sulphate-reducing magnetotactic bacterium *Desulfovibrio magneticus* RS-1. *Proteomics* 9:3341–3352.
26. Grünberg K, et al. (2004) Biochemical and proteomic analysis of the magnetosome membrane in *Magnetospirillum gryphiswaldense*. *Appl Environ Microbiol* 70: 1040–1050.
27. Arakaki A, Webb J, Matsunaga T (2003) A novel protein tightly bound to bacterial magnetic particles in *Magnetospirillum magneticum* strain AMB-1. *J Biol Chem* 278: 8745–8750.
28. Murat D, Quinlan A, Vali H, Komeili A (2010) Comprehensive genetic dissection of the magnetosome gene island reveals the step-wise assembly of a prokaryotic organelle. *Proc Natl Acad Sci USA* 107:5593–5598.
29. Amemiya Y, Arakaki A, Staniland SS, Tanaka T, Matsunaga T (2007) Controlled formation of magnetite crystal by partial oxidation of ferrous hydroxide in the presence of recombinant magnetotactic bacterial protein Mms6. *Biomaterials* 28: 5381–5389.
30. Scheffel A, Gärdes A, Grünberg K, Wanner G, Schüler D (2008) The major magnetosome proteins MamGFDC are not essential for magnetite biomineralization in *Magnetospirillum gryphiswaldense* but regulate the size of magnetosome crystals. *J Bacteriol* 190:377–386.
31. Hanzlik M, Winklhofer M, Petersen N (2002) Pulsed-field-remanence measurements on individual magnetotactic bacteria. *J Magn Magn Mater* 248:258–267.
32. Guerquin-Kern JL, Wu TD, Quintana C, Croisy A (2005) Progress in analytical imaging of the cell by dynamic secondary ion mass spectrometry (SIMS microscopy). *Biochim Biophys Acta* 1724:228–238.
33. Azari F, et al. (2008) Intracellular precipitation of hydroxyapatite mineral and implications for pathologic calcification. *J Struct Biol* 162:468–479.